ORIGINAL RESEARCH ARTICLE

Effect of Heating Temperature on Microstructures and Tribological Properties of Near βTi Alloy

Bo Song, Yisen Wang, Wenlong Xiao, Chaoli Ma, Lian Zhou, Yanbiao Ren, Ruipu Li, Hui Chen, Hongyang Wang, Tianwen Zhen, Jiamu Fu, and Baoyu Shi

The influence of heating temperature on microstructures and tribological properties of near βTi alloy Ti-5Al-3Mo-3V-2Cr-2Zr-1Nb-1Fe (wt.%) has been studied in this work. The volume fraction of primary α decreases gradually with solution temperature increasing, and as a result, the hardness and wear resistance are reduced. After aging treatment, the wear resistance of alloy is obviously improved. During aging the secondary α precipitates coarsen with aging temperature increasing. Secondary α precipitates are more effective to strengthen alloy than primary α. During friction process with stainless steel, the wear mechanisms of aged samples are mixture of abrasive wear, adhesive wear, and oxidation wear. Thermodynamic calculation by JmatPro software shows that the thickness growth rate (v) of α precipitates and aging temperature (T) obey the formula of $v = 489.1936 \times 10^{0.0424}\ T$, which is evidenced by experimental results. The transformation of α phase from β is corresponded with the BOR relationships, $\{110\}_\beta//\{0001\}_\alpha$ and $[111]_\beta//[11\bar{2}0]_\alpha$.

1. Introduction

Near βTi alloy has been widely used in aerospace field as structural material due to the low density, high specific strength and excellent corrosion resistance (Ref 1-3). It belongs to age-hardenable alloy. The α precipitation from β phase matrix during aging will lead to larger strength and hardness in comparison with solution-treated state (Ref 4). It has been well known that the morphology, size, volume fraction and distribution of α phase greatly affect such precipitation hardening effect (Ref 5, 6). Through tailoring heat treatments, the features of α precipitates will be changed apparently, and the strength and ductility of alloy fluctuate in a wide range (Ref 7, 8).

It has been reported in the literature that various heat treatments have been employed to control α precipitation, i.e., slow heating to aging temperatures and dual-aging treatments (Ref 9-12). It is suggested that increasing primary α phase quantity is beneficial to improve ductility of alloy, and a dense and uniform distribution of fine secondary α precipitates contributes to high strength. Therefore, bimodal microstructure consisting of both primary α and secondary α should achieve better comprehensive mechanical properties in comparison with the others. Du. et al. (Ref 13) studied the microstructures and properties of Ti-3.5Al-5Mo-6V-3Cr-2Sn-0.5Fe alloy with different microstructures, and they found that the (α + β) zone solution-treated samples showed higher strength after aging than the β solution-treated one. Shashi Shekhar et al. (Ref 14) found that Ti-5553 alloy obtained higher strength and ductility by developing bimodal microstructure. However, the formation of primary α can actually influence secondary α precipitation behavior, since the primary α volume fraction increment will reduce the driving force for secondary α nucleation and growth.

Tribological properties of Ti alloys have been carefully examined previously due to their usage. Unfortunately, most studies concentrated on (α + β) Ti alloy, such as Ti-6Al-4 V, and researches on the near βTi alloy are limited. Generally, the βTi alloy has acceptable wear resistance, and it has been found that cryogenic treatment can improve its tribological properties (Ref 15, 16). We know that the mechanical properties of near βTi alloys are closely related to their microstructures. Therefore, the relationships between microstructures and tribological properties are studied in this work using near βTi alloy Ti-5Al-3Mo-3V-2Cr-2Zr-1Nb-1Fe (wt.%, Ti-5321). This alloy is firstly developed to manufacture landing gear, fasteners and connectors in aerospace field. Tensile properties of this alloy have been examined previously (Ref 17, 18), and its ultimate tensile strength, total elongation and fracture toughness fluctuate in a range of 1147-1439 MPa, 3-26% and 57-76 MPa m$^{1/2}$, respectively. It is found that this alloy is also suitable to aerospace environmental control system ducting recently, which requires excellent wear resistance. However, little information on the

Bo Song, School of Materials Science and Engineering, Liaocheng University, Liaocheng 252059 Shandong, China; and Key Laboratory of Aerospace Advanced Materials and Performance of Ministry of Education, School of Materials Science and Engineering, Beihang University, Beijing 100191, China; **Yisen Wang, Ruipu Li, Hui Chen, Hongyang Wang, Tianwen Zhen, Jiamu Fu,** and **Baoyu Shi**, School of Materials Science and Engineering, Liaocheng University, Liaocheng 252059 Shandong, China; **Wenlong Xiao, Chaoli Ma,** and **Lian Zhou**, Key Laboratory of Aerospace Advanced Materials and Performance of Ministry of Education, School of Materials Science and Engineering, Beihang University, Beijing 100191, China; and **Yanbiao Ren**, College of Chemistry, Chemical Engineering and Materials Science, Zaozhuang University, Zaozhuang 277160 Shandong, China. Contact e-mails: songbo@lcu.edu.cn and wlxiao@buaa.edu.cn.

relationships between microstructures and tribological properties of Ti-5321 alloy is reported. Therefore, the influence of heat treatments on wear resistance of Ti-5321 alloy needs to be studied in detail, as well as its wear mechanisms.

2. Materials and Methods

This alloy was supplied by Northwest Institute for Non-ferrous Metal Research, China (Ref 17, 18). The ingot was prepared by vacuum arc melting and hot-rolled in (α + β) zone into ϕ 20 mm cylinders. Its [Mo] value was 6.05, and the α/β transformation temperature was 860 ± 5 °C. Based on d-electron theory, its Bo and Md values were 2.77 and 2.37, respectively.

Some samples were solution-treated at 800, 820 and 840 °C for 1 h, and the others were solution-treated at 900 °C for 0.5 h, followed by water quenching. After solution treating, these samples were put into furnace preheated to aging temperatures,
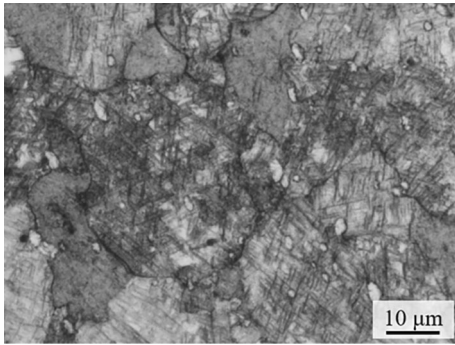

Fig. 1 OM micrograph showing initial microstructure of Ti-5321 alloy

i.e., 530, 570, 600 and 650 °C, and isothermally aged for 8 h followed by water quenching. To study the growth of α precipitates upon aging at 600 °C, the aging treatment was interrupted at 0.5, 1, 3 and 5 h by water quenching. All treatments were performed with Ar atmosphere protection. When aging heat treatments finished, these samples were ground, polished and etched for microstructural observation. Standard Kroll's reagent (10 ml HF + 30 ml HNO$_3$ + 70 ml H$_2$O) was utilized to reveal microstructures. The α phase was observed by optical microscopy (OM) and scanning electron microscopy (SEM). The phase constituents of samples were identified by x-ray diffraction (XRD). The average length, thickness and number density of α phase were obtained by Image-Pro Plus software. Thermodynamic calculation by JmatPro software was conducted to study the growth kinetics of α precipitates upon aging. The microhardness was measured at a load of 9.8 N for 10 s. Ten points were tested for each sample. Tribological properties were evaluated by wear tests under dry sliding condition. All wear tests were performed at room temperature in air using stainless steel ball (ϕ = 6 mm) under conditions of 5 mm scratch length, 2 N applied load, 0.02 m/s fixed sliding velocity, 2 Hz frequency and 12 min sliding time. The wear rate (W) was calculated by the formula of $W = V/(F{\cdot}L)$, where V was the wear volume loss, L the total sliding distance and F the applied load.

3. Results

3.1 Microstructures

OM micrograph showing the microstructure of Ti-5321 alloy in hot-rolled state is given in Fig. 1, which is composed of equiaxed α, acicular α and martensite. Similar observations have been reported by Wu et al. (Ref 19). It is found that the volume fraction of primary α is decreasing gradually with
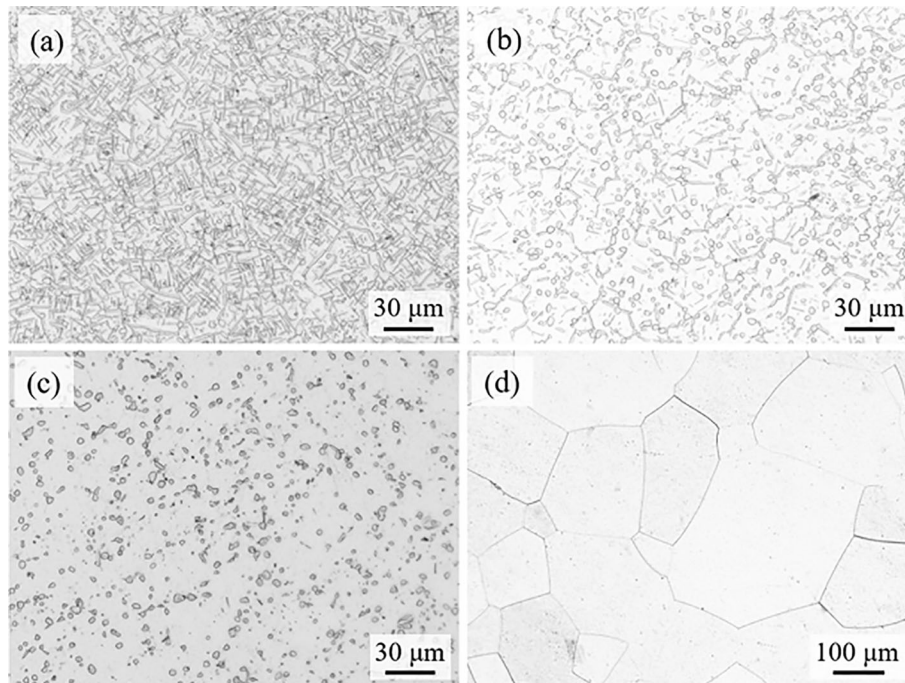

Fig. 2 Microstructures of the samples solution treated at (a) 800, (b) 820, (c) 840 and (d) 900 °C
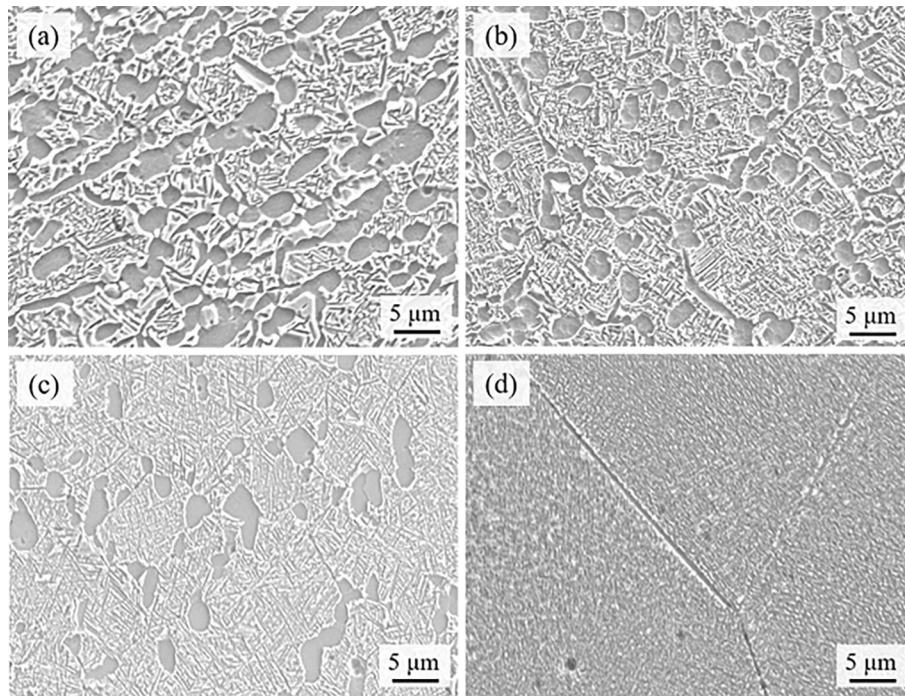
Fig. 3 SEM images showing the distribution of secondary α precipitates in the samples aged at 650 °C after solution-treated at (a) 800, (b) 820, (c) 840 and (d) 900 °C
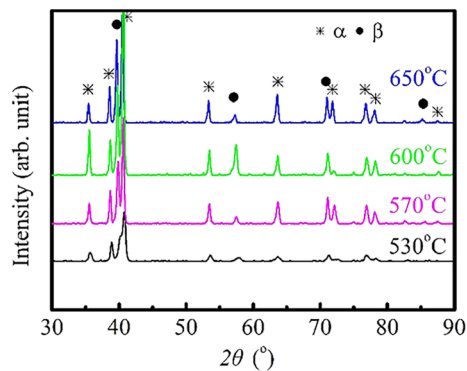

Fig. 4 XRD patterns of the β-quenched sample after aging at different temperatures

solution temperature increasing (Fig. 2). Both plate-shaped and equiaxed primary α phase can be observed at solution temperatures of 800 and 820 °C. When solution-treated at 840 °C, those plate-shaped α phases vanish completely. The volume fraction of primary α in the samples solution at 800, 820 and 840 °C is $65 \pm 8\%$, $47 \pm 11\%$ and $25 \pm 5\%$, respectively. For the sample solution at 900 °C, the microstructure of β grains is formed. After aging at 650 °C, bimodal microstructures are developed in the samples solution treated below 860 °C shown in Fig. 3(a), (b), and (c). For the β solution-treated and aged sample, a dense and uniform distribution of fine α precipitates is observed (Fig. 3d).

XRD results showed that α and β phases co-exist in the aged samples (Fig. 4). For the β solution-treated samples, the α precipitates exhibit short-rod shape during aging (Fig. 5). Due to excessive etching, some black spots appear. With the aging temperature increasing, the average thickness of α precipitates increases gradually, and their number density decreases corre-

spondingly. The features of α precipitates are summarized in Table 1.

3.2 Hardening Effect

The hardness of these samples is given in Fig. 6(a). With the solution temperature increasing from 800 to 900 °C, the hardness of alloy decreases gradually from 213 ± 2 to 198 ± 4 HV. Upon aging at 650 °C, secondary α precipitates are formed and result in strong precipitation hardening effect. The aged samples have higher hardness than the solution-treated ones. It is found that the hardness of aged samples increases gradually at first and then decreases with solution temperature increasing. The largest hardness (268 ± 11 HV) is obtained at 840 °C. For the samples solution treated at 800, 820 and 900 °C, their hardness values are 254 ± 9, 259 ± 10 and 259 ± 15 HV, respectively. To clarify the influence of α precipitates, the hardness of the β solution-treated sample aged at different temperatures is tested. It shows that the hardness of samples decreases gradually with the aging temperature increasing (Fig. 6b). The hardness of samples aged at 530, 570 and 600 °C is 362 ± 6, 315 ± 15 and 281 ± 13 HV, respectively.

3.3 Tribological Properties

The wear behaviors of samples solution at various temperatures are shown in Fig. 7. It is noted that the friction coefficient curve of the sample solution at 840 °C fluctuates with test time prolonging, and the others are more stable. It is observed that the average friction coefficients of the samples solution at 800 and 820 °C seem to be same, but it increases suddenly at 840 °C. This indicates that the wear behavior changes when solution temperature increases from 820 to 840 °C. This should be mainly due to the plate-shaped α phase disappearance and the equiaxed α amount reduction. The wear ratios of the
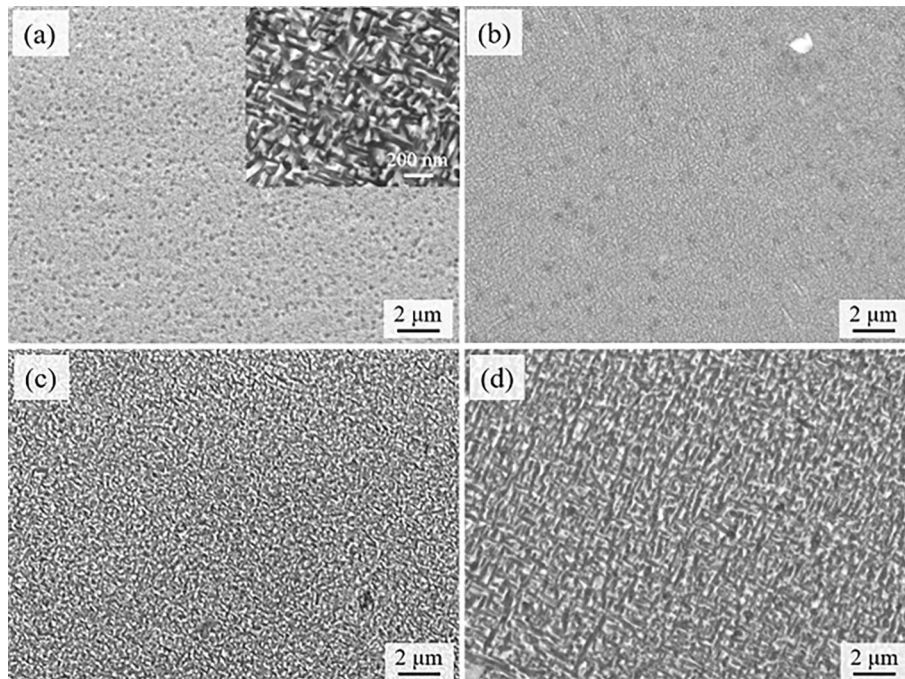
Fig. 5 SEM images showing the microstructures of β solution-treated samples aged at (a) 530, (b) 570, (c) 600 and (d) 650 °C

Table 1   Features of α phase in β-quenched samples after aging at different temperatures

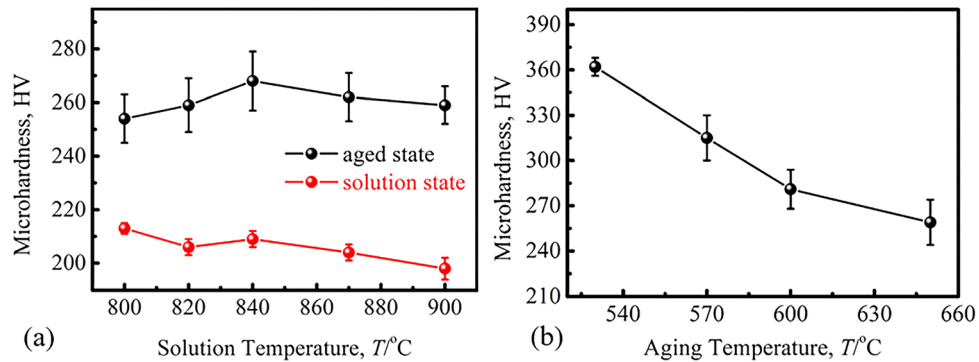|	Thickness, μm	Length, μm	Aspect ratio	Number density, laths/μm²
530, °C	0.009 ± 0.003	0.023 ± 0.01	2.6 ± 0.2	25 ± 2
570, °C	0.1 ± 0.02	0.27 ± 0.08	2.7 ± 0.8	17 ± 3
600, °C	0.14 ± 0.03	0.4 ± 0.1	2.9 ± 0.5	14 ± 2
650, °C	0.22 ± 0.05	0.88 ± 0.2	4.0 ± 0.5	5 ± 1

Fig. 6 Hardness of the samples solution at different temperatures when aged at 650 °C (a) and (b) the hardness of β-quenched sample aged at different temperatures

samples solution at various temperatures are also comparatively studied. With solution temperature increasing from 800 to 900 °C, it increases continuously up to 15.30 × 10^{-6} mm³/ (N m). In comparison with the solution samples, the aged ones exhibit better tribological properties. The wear ratio of alloy is greatly reduced after aging (Fig. 8) because the secondary α precipitates formation results in great hardening effect.

In order to study the wear behaviors of aged samples, friction coefficient curves of the samples solution at various temperatures and aged at 650 °C are plotted in Fig. 9(a), and their average friction coefficients and wear ratios are calculated. With the solution temperature increasing, the friction coefficients decreases at first and then increases. The sample solution treated at 840 °C has the best tribological properties. When the solution temperature increases from 800 to 840 °C, the friction
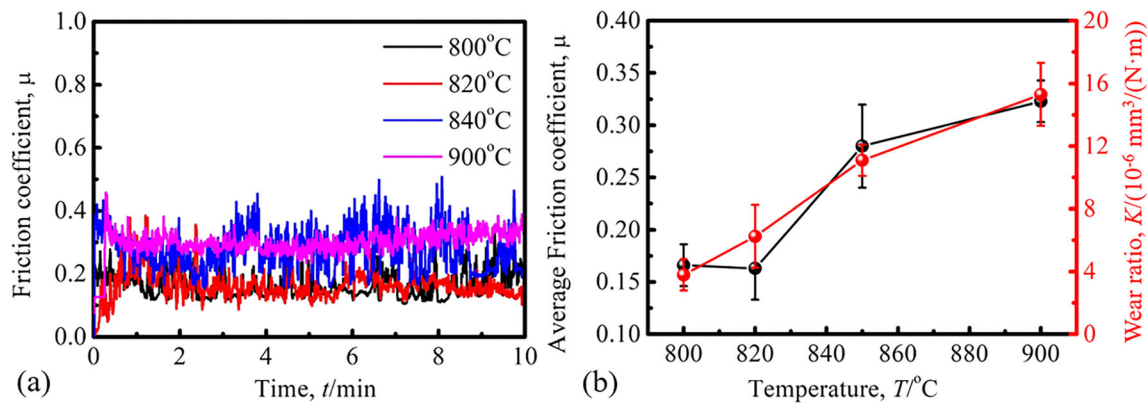
Fig. 7 Friction coefficient curves (a) and (b) wear trace volumes for the samples solution at different temperatures
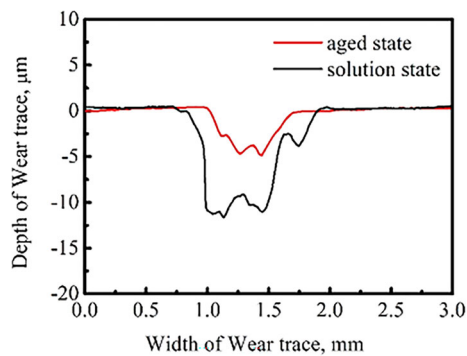

Fig. 8 Comparison of the wear loss volumes in β-quenched sample before and after aging

coefficient decreases from 0.406 ± 0.065 to 0.113 ± 0.027, and the wear ratio decreases from 5.7 to 2.55×10^{-6} mm^3/(N·m). For the sample solution at 900 °C, its friction coefficient and wear ratio grow up to 0.301 ± 0.05 and 6.65×10^{-6} mm^3/(N·m), respectively.

To evaluate the influence of secondary α precipitates to the wear resistance of alloy, the friction coefficient curves of the β-quenched samples after aging at various temperatures are plotted in Fig. 10(a). It is noted that the friction coefficient and wear ratio of samples fluctuate with the aging temperature increasing from 530 to 600 °C (Fig. 10b). Once the aging temperature increases up to 650 °C, the wear ratio of alloy increases greatly. Therefore, it is thought that this alloy has acceptable wear resistance when aged below 600 °C.

Typical worn surface morphology of these aged samples is given in Fig. 11(a) and (b). It presents plenty of grooves and abrasive debris. Upon the friction process, the load is transmitted through the normal and tangential directions of contact points, leading to normal stress and shear stress generation. Under the effect of normal stress, the friction contact surface will be scratched and plowed out grooves. Due to the comparatively low shear resistance of Ti alloy, adhesion and tearing are likely to appear on worn surface. Several micro-pits and micro-furrows are observed on the worn scar surface, which is referred by red contrast in Fig. 11(b). This indicates typical abrasive wear. The wear scar surface of the samples is

very rough with deep furrows and layered structures form by shearing, which suggests that the adhesive wear occurs. The XRD spectra in Fig. 11(d) show the formation of TiO$_2$, Al$_2$O$_3$ and Fe$_2$O$_3$ on the wear scar surface during friction process. The O, Al, Ti and Fe atoms distribution further evidences the formation of these oxides (Fig. 11e-h). Therefore, oxidation reaction actually occurs during friction. Severe plastic deformation happened during wear tests can result in numbers of dislocations multiplication and entanglement. As a result, microcracks nucleate and peel off repeatedly, leading to the abrasive debris formation. It is in nature an abrasive wear and adhesive wear mixed process. Therefore, the wear mechanisms of this alloy mainly include abrasive wear, adhesive wear, and oxidation wear.

4. Discussion

It is thought that the secondary α precipitates play a more important role in affecting wear resistance of alloy than primary α. The aged samples obtain better wear resistance in comparison with the solution-treated ones. When dislocations encounter with α/β interfaces and β grain boundaries during wear test, they will accumulate and tangle leading to dislocations enriched regions. After aging treatment, a uniform distribution of fine secondary α precipitates is developed, which produces plenty of α/β interfaces hindering dislocations slipping. This should be the reason why secondary α precipitates are more useful to strengthen alloy.

As discussed previously (Ref 20, 21), the nucleation of α precipitates in this alloy is via O'-assisted mechanism upon aging. There are three intermediate phases (O', ω and O'') formation before α nucleation, and the α precipitates are observed when the sample is heated to 430 °C. At this temperature, the ω and O'' phases disappear, and only O' phase still exists. The O' phase with orthorhombic structure is developed by the $\{110\}_\beta[1 \bar{1} 0]_\beta$ shuffle mechanism, and it has six variants. The relationships between O' and β lattice parameters are $a_{O''} = a_\beta$, $b_{O'} = \sqrt{2}\, a_\beta$ and $c_{O'} = \sqrt{2}\, a_\beta$, and the orientation relationships between two phases obey $[001]_\beta(0 \bar{1} 1)_\beta//[100]_{O'}(020)_{O'}$, $[110]_\beta(002)_\beta//[001]_{O'}(200)_{O'}$, $[111]_\beta(1 \bar{1} 0)_\beta//[110]_{O'}(002)_{O'}$, $[113]_\beta(1 \bar{1} 0)_\beta//[1 \bar{1} 2]_{O'}(1 \bar{1}\bar{1})_{O'}$. As
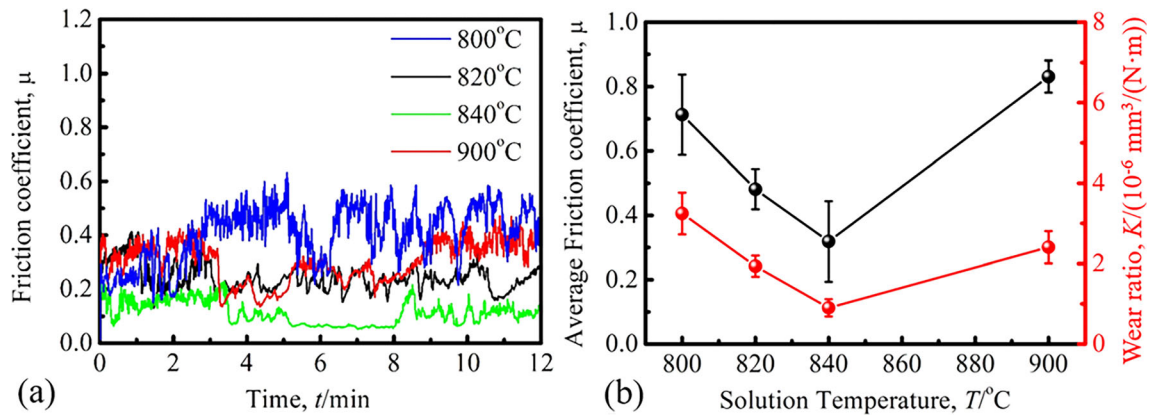
Fig. 9 Friction coefficient curves (a) and (b) mass loss ratios of samples aged at 650 °C after solution-treated at different temperatures
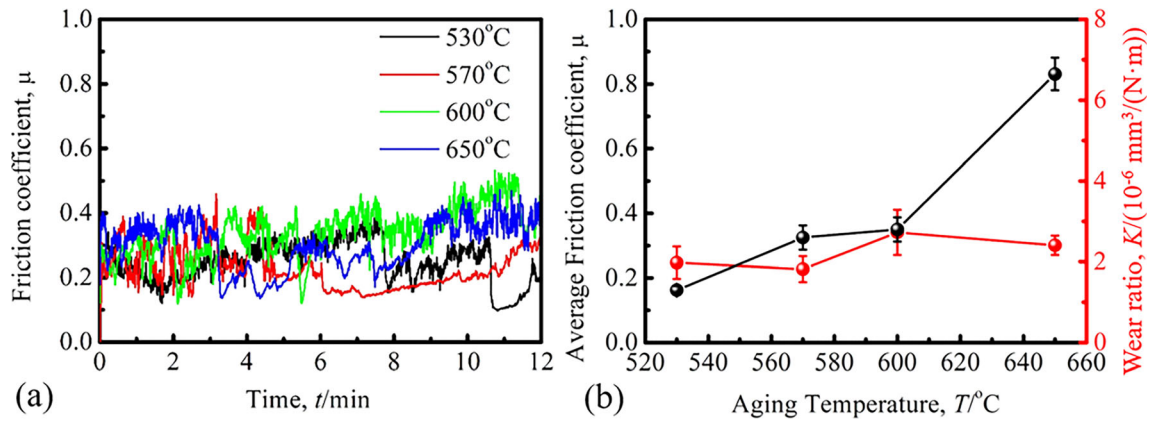

Fig. 10 Friction coefficient curves (a) and (b) mass loss ratios of the β-quenched sample after aging at different temperatures

reported, the isothermal ω phase having HCP structure is transformed by via a diffusion-mediated process, and the atoms on $\{111\}_\beta$ planes collapse along $[111]_\beta$ direction. The O″ phase with ordered face-centered orthorhombic structure is transformed at intermediate temperature ranges in β Ti alloy. Ordering occurs every three $\{001\}_{O''}$ atom planes. For the Ti-5321 alloy in this work, the ω and O″ phases will disappear before α precipitation, and the O′ domains directly promote α phase formation. While the transformations of ω and O″ are closely related to the formation of O′ domains, it is suggested that the ω and O″ play indirect role in promoting α nucleation. It is known that the solute atoms will be excluded from isothermal ω upon aging. This can facilitate the O′ domains development in the regions nearby ω, and such proximity of O′ and ω has been observed in Ti-23Nb-2O alloy in Ref 22. The O″ structure is thought can be formed within O′ phase, due to their coherent interface and low misfit. It is found that the lattice parameters between O′ and O″ obey $a_{O'} = a_{O''}$, $b_{O'} = b_{O''}$ and $c_{O''} = 3c_{O''}$.

Even though three intermediate phases are developed, only the O′ phase can be retained when α phase nucleates. The O′ phase is continuously formed during α precipitation. The α phase tends to nucleate at O′/β phase interfaces, which can greatly reduce energy obstacle for α precipitation. The α needles are inclined to form at the O′/β phase interfaces. The phase transformation sequence in Ti-5321 alloy upon continuous heating is $\beta + \omega_{embryo} + O' \rightarrow \beta + \omega_{iso} + O' \rightarrow \beta + \omega_{iso}$ $+ O' + O'' \rightarrow \beta + O' + \alpha \rightarrow \beta + \alpha$. Experimental observations have been shown in Ref 21. It is reported in the literature that the interfaces between metastable phases and β matrix can facilitate α precipitation, because they act as favorable nucleation sites for α and decrease the energy barrier for α nucleation in β (Ref 23, 24). For Ti-5321 alloy, the O′ domains provide additional heterogeneous nucleation site for α; hence, it is suggested that the α nucleation upon aging treatment in this alloy is via O′-assisted mechanism. When the aging heating rate ranged from 0 to 100 °C/min, a dense and uniform distribution of fine α precipitates can always be formed. It is thought that the microstructures and mechanical properties of this alloy are not sensitive to such aging heating rate, since plenty of O′ domains can always be formed and provide additional effective nucleation site for α precipitation. Because the nucleation of α phase has been discussed before, in this work we mainly focus on studying the growth of α precipitates during aging by theoretical and experimental methods.

Through JmatPro software calculation, the equilibrium concentration of elements in α and β phases at different aging temperatures is obtained (Fig. 12). Detailed introduction of this software is reported in Ref 25. The content of β-stabilizers in β phase slowly decreases, and the content of Al element climbs up with aging temperature increasing. The content of alloy elements in α phase seems to be independent on aging temperature. Through the JmatPro software simulation, the
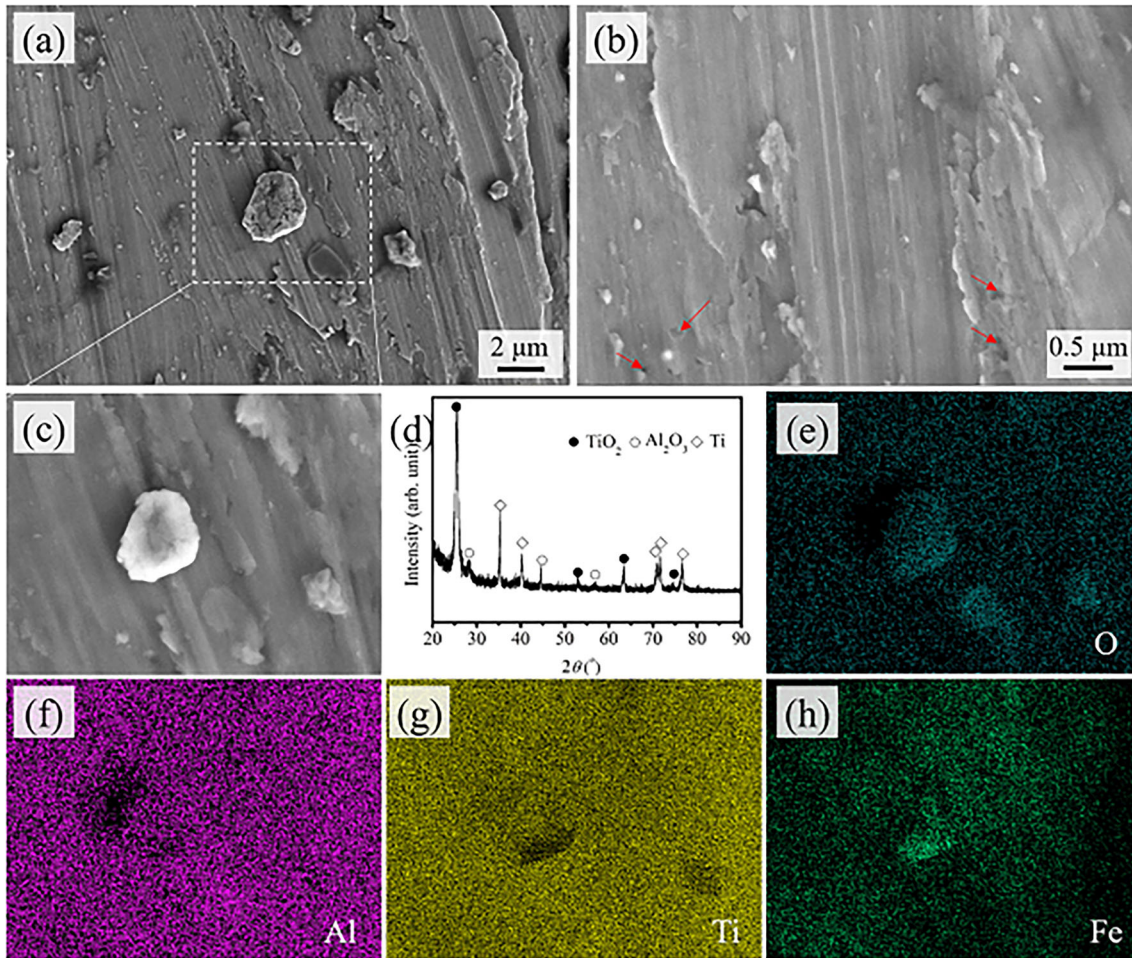
Fig. 11 SEM images (a-c) showing the typical worn scar surface of aged samples, and (d) XRD analysis of the oxidation. EDS results (e-h) presenting the O, Al, Ti and Fe atoms distribution on worn surface
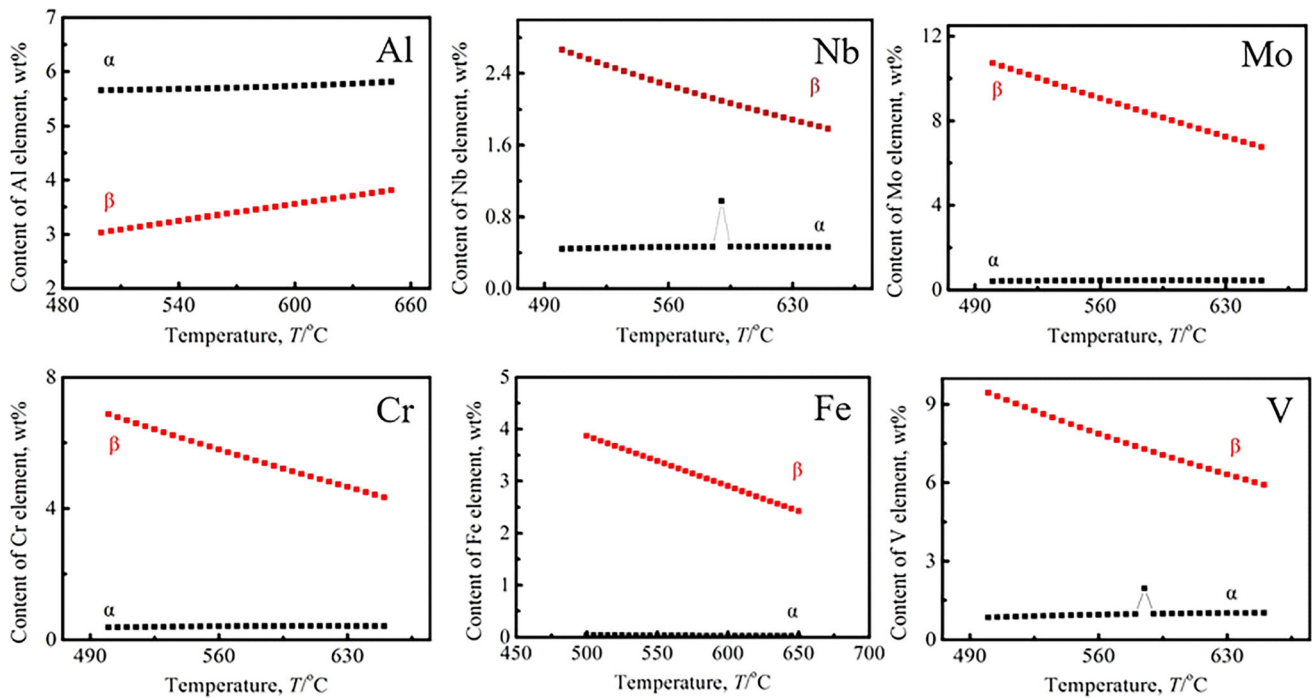

Fig. 12 Calculated content of alloy elements in α and β upon aging at different temperatures

equilibrium phase chemical composition can be calculated automatically when the aging temperature and alloy composition are given. Because there are seven alloy elements, [Mo] value is calculated and regarded as the phase composition. The [Mo] values are calculated by the equation of [Mo] = w(Mo) + w(Nb) × 0.28 + w(Fe) × 2.9 + w(V)×0.67 + w(Cr) × 1.6, where w is the weight fraction of various elements. [Mo] values of α and β at different aging temperatures are shown in Table 2.

Table 2 The [Mo] values of α and β phases at different aging temperatures by JmatPro software simulation

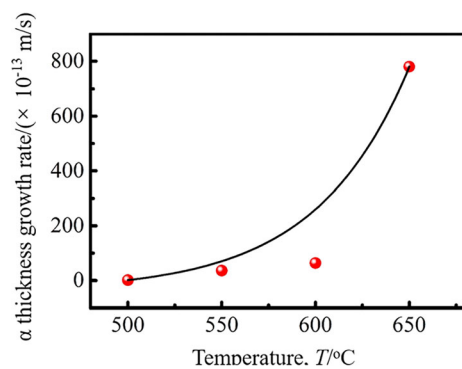|	500, °C	550, °C	600, °C	650, °C
$C_{[Mo]}^{\alpha}$	1.68	1.85	1.91	2.0
$C_{[Mo]}^{\beta}$	39.9	34.8	29.8	25.2

Fig. 13 Growth rate of α precipitate in β-quenched samples upon aging at different temperatures

Based on Arrhenius equation and Zener formula, the thickness growth rates of α precipitates at various aging temperatures are calculated and plotted in Fig. 13. The α thickness growth rate v is calculated by the formula (1) of

$$v = \frac{D}{C_{[Mo]}^{\beta} - C_{[Mo]}^{\alpha}} \cdot \frac{C_{[Mo]}^{alloy} - C_{[Mo]}^{\alpha}}{L}$$

where $C_{[Mo]}^{\alpha/\beta}$ is the [Mo] values of α or β, $C_{[Mo]}^{alloy}$ the [Mo] value of this alloy, D the atomic diffusion coefficient, and L the atomic diffusion distance. The atomic diffusion coefficient D is calculated by $D = D_0 e^{(-Q/RT)}$, in which Q is the diffusion activation energy of Mo atoms 147.353 kJ/mol, R the gas constant 8.314 J/(mol·K), T the aging temperature, and D_0 the diffusion constant of Mo atoms. As reported in Ref 25, the atomic diffusion coefficients D in β Ti alloy are 1.113, 2.794, 4.079 and 3.974 × 10^{-13} m²/s at 500, 550, 600 °C and 650 °C, respectively. The atomic diffusion distance L is 1 μm obtained from Ref 25, because it nearly equals to the tip curvature radius of α precipitates. When we substitute data in Table 2 and the atomic diffusion coefficients into the formula (1), the α thickness growth rate v can be obtained shown in Fig. 12. Some abnormal points of V and Nb can be ignored because they will not influence final results. The appearance of such abnormal points may be resulted by the JmatPro software simulation. When the alloy is aged at 500, 550 and 600 °C, the thickness growth rates of α precipitates are 1.34, 36.12 and 63.71 × 10^{-13} m/s, respectively. When aging temperature increased to 650 °C, the α precipitates thickness growth rate increases to 7.8 × 10^{-11} m/s. As a result, the relationship between α thickness growth rate (v) and aging temperature (T) is obtained $v = 489.1936 × 10^{0.0424}\ T$.

To prove the efficiency of this relationship, the α precipitates in the β solution-treated sample during aging at 600 °C for different times are observed (Fig. 14). When aged for 0.5 h, the thickness, length and number density of α precipitates are
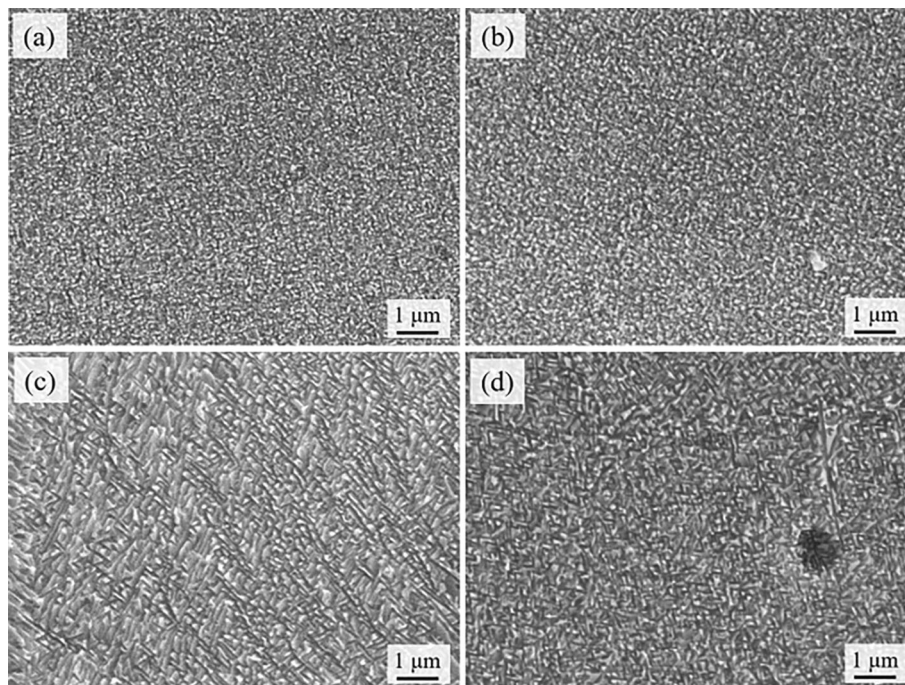
Fig. 14 SEM images showing the α precipitates in β-quenched samples during aging at 600 °C for (a) 0.5, (b) 1, (c) 3 and (d) 5 h

Table 3 Features of α precipitates upon aging at 600 °C for various times

	Thickness, μm	Length, μm	Aspect ratio	Number density, laths/μm^2
0.5, h	0.06 ± 0.01	0.23 ± 0.07	3.8 ± 0.8	26 ± 1
1, h	0.08 ± 0.02	0.2 ± 0.05	2.5 ± 0.2	25 ± 5
3, h	0.12 ± 0.03	0.33 ± 0.08	2.8 ± 0.5	20 ± 3
5, h	0.13 ± 0.04	0.38 ± 0.02	2.4 ± 0.2	16 ± 5
8, h	0.14 ± 0.03	0.4 ± 0.1	2.9 ± 0.5	14 ± 2
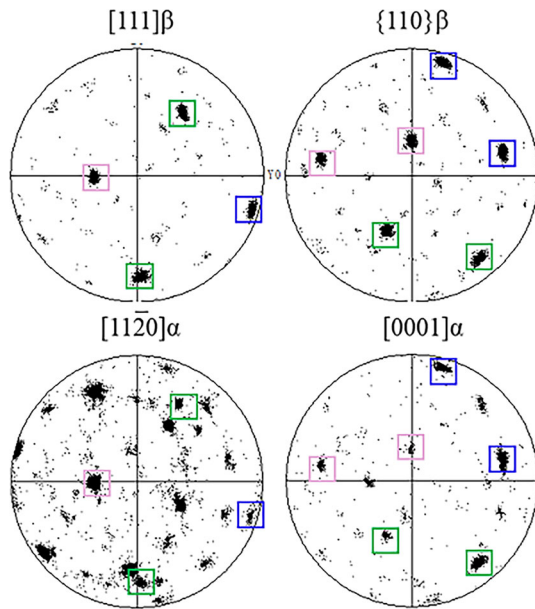
Fig. 15 EBSD pole figure illustrating orientation relationships between α and β phases

measured to be 0.06 ± 0.01 μm, 0.23 ± 0.07 μm and 26 ± 1 laths/μm^2, respectively. With the aging time prolonging to 5 h, its average thickness and length increase to 0.14 ± 0.03 and 0.4 ± 0.1 μm, and the number density is reduced to 14 ± 2 laths/μm^2. The features of α precipitates are concluded in Table 3. It is noticed that the experimental growth rate of α thickness is 45×10^{-13} m/s at 600 °C. As mentioned above, the calculated growth rate of α phase thickness during aging at 600 °C is 63.71×10^{-13} m/s. The experimental result is slightly smaller than the calculated one. It is thought that such difference should be because the experimental growth rate of α phase is measured from the aging time of 0.5 h. The driving force for α precipitation has been reduced in comparison with initial β-quenched state; therefore, lower growth rate of α phase thickness is obtained. Based on EBSD analysis (Fig. 15), it is found that the transformation of α precipitates from parent β matrix obeys BOR orientation relationships, $\{110\}_\beta//\{0001\}_\alpha$ and $[111]_\beta//[11\bar{2}0]_\alpha$.

5. Conclusions

In this work the influence of heating temperatures on microstructures and tribological properties of Ti-5321 alloy is researched. The results are concluded below:

(1) With solution temperature increasing, the amount of primary α decreases gradually. Secondary α precipitates are coarsened during aging with the aging temperature increasing. The precipitation of secondary α obeys BOR orientation relationships with β matrix, $\{110\}_\beta//\{0001\}_\alpha$ and $[111]_\beta//[11\bar{2}0]_\alpha$.

(2) For the β solution-treated alloy, the relationship between α phase thickness growth rate v and aging temperature T is $v = 489.1936 \times 10^{0.0424} T$, which is obtained by JmatPro software simulation and being corresponding experimental results.

(3) In comparison with solution sample, the aged sample has better wear resistance. During wear testing, the abrasive wear, adhesive wear and oxidation wear are main wear mechanisms. When solution-treated at 840 °C and aged at 650 °C, the sample exhibits best wear resistance, and its hardness, friction coefficient and wear ratio are 268 ± 11 HV, 0.113 ± 0.027 and 2.55×10^{-6} mm^3/(N·m), respectively.

Conflict of interest

The authors declare that they have no known competing financial interests or personal relationships that could have appeared to influence the work reported in this paper.

References

1. Q.Y. Zhao, Q. Sun, S. Xin, Y. Chen, C. Wu et al., High-Strength Titanium Alloys for Aerospace Engineering Applications: A Review on Melting-Forging Process, *Mater. Sci. Eng. A*, 2022, **845**, 143260

2. N. Yumak and K. Aslantaş, A Review on Heat Treatment Efficiency in Metastable β Titanium Alloys: The Role of Treatment Process and Parameters, *J. Mater. Sci. Technol.*, 2020, **9**, p 15360–15380.

3. J.D. Cotton, R.D. Briggs, R.R. Boyer, S. Tamirisakandala, P. Russo et al., State of the Art in Beta titanium Alloys for Airframe Applications, *JOM*, 2015, **67**, p 1281–1303.

4. C.P. Zhu, X.Y. Zhang, C. Li, C.Q. Liu, and K.C. Zhou, A Strengthening Strategy for Metastable β Titanium Alloys: Synergy Effect of primary α Phase and β Phase Stability, *Mater. Sci. Eng. A*, 2022, **852**, 143736

5. H.Y. Zhang, C. Wang, G. Zhou, S.Q. Zhang, and L.J. Chen, Dependence of Strength and Ductility on Secondary α Phase in a Novel Metastable-β Titanium Alloy, *J. Market. Res.*, 2022, **18**, p 5257–5266.

6. Y. Liu, S.C.V. Lim, C. Ding, A. Huang, and M. Weyland, Unravelling the Competitive Effect of Microstructural Features on the Fracture Toughness and Tensile Properties of Near Beta Titanium Alloys, *J. Mater. Sci. Technol.*, 2022, **97**, p 101–112.

7. W. Zhu, J. Lei, C. Tan, Q. Sun, W. Chen, L. Xiao, and J. Sun, A Novel High-Strength β-Ti Alloy with Hierarchical Distribution of α-Phase: The Superior Combination of Strength and Ductility, *Mater. Des.*, 2019, **168**, 107640

8. X. Li, X. Wang, K. Liu, J.Y. Wang, X. Guo, M.B. Li, Z.S. Zhu, and S.J. Wu, Microstructure evolution and Mechanical Property of a New Multi-Component β Titanium Alloy with Ultrahigh Strength Above 1350 MPA, *J. Market. Res.*, 2022, **21**, p 4860–4875.

9. J. Zhang, H. Ju, H. Xu, L. Yang, Z. Meng, C. Liu, P. Sun, J. Qiu, C. Bai, D. Xu, and R. Yang, Effects of Heating Rate on the Alloy Element Partitioning and Mechanical Properties in Equiaxed α+β Ti-6Al-4V Alloy, *J. Mater. Sci. Technol.*, 2021, **94**, p 1–9.

10. M.G. de Mello, B.P. Dainese, R. Caram, and A. Cremasco, Influence of Heating Rate and Aging Temperature on Omega and alpha Phase Precipitation in Ti 35Nb Alloy, *Mater Charact*, 2018, **145**, p 268–276. https://doi.org/10.1016/j.matchar.2018.08.035

11. C.J. Zhang, X. Jiang, Z.D. LÜ, H. Feng, S.Z. Zhang, Y. Xu, M.D. Hayat, and P. Cao, Effect of Duplex Aging on Microstructure and Mechanical Properties of near-β Titanium alloy Processed by Isothermal Multidirectional Forging, *Trans. Nonferrous Metals Soc. China*, 2022, **32**, p 1159–1168.

12. C.A.F. Salvador, V.C. Opini, M.G. Mello, and R. Caram, Effects of Double-Aging Heat-Treatments on the Microstructure and Mechanical Behavior of an Nb-Modified Ti-5553 Alloy, *Mater. Sci. Eng. A*, 2019, **743**, p 716–725. https://doi.org/10.1016/j.msea.2018.11.086

13. Z.X. Du, S.L. Xiao, L.J. Xu, J. Tian, F. Kong, and Y. Chen, Effect of Heat Treatment on Microstructure and Mechanical Properties of a New β High Strength Titanium Alloy, *Mater. Des.*, 2014, **55**, p 183–190.

14. S. Shekhar, R. Sarkar, S.K. Kar, and A. Bhattacharjee, Effect of Solution Treatment and Aging on Microstructure and Tensile Properties of High Strength β Titanium Alloy, Ti–5Al–5V–5Mo–3Cr, *Mater. Des.*, 2015, **66**, p 596–610.

15. S. Guo, Q. Zheng, X.L. Hou, X.N. Cheng, and X.Q. Zhao, Wear Response of Metastable β-type Ti–25Nb–2Mo–4Sn alloy for Biomedical Applications, *Rare Met.*, 2015, **34**, p 564–568.

16. K.X. Gu, J. Wang, and Y. Zhou, Effect of Cryogenic Treatment on Wear Resistance of Ti–6Al–4V Alloy for Biomedical Applications, *J. Mech. Behav. Biomed. Mater.*, 2014, **30**, p 131–139.

17. L. Ren, W. Xiao, H. Chang, Y. Zhao, C. Ma, and L. Zhou, Microstructural Tailoring and Mechanical Properties of a Multi-Alloyed Near β Titanium Alloy Ti-5321 with Various Heat Treatment, *Mater. Sci. Eng. A*, 2018, **711**, p 553–561.

18. Y.Q. Zhao, C.L. Ma, H. Chang, and L. Zhou, New High Strength and High Toughness Titanium Alloy with 1200 MPa, *Mater. China*, 2016, **35**, p 914–917.

19. C. Wu, Q.Y. Zhao, S. Huang, Y. Zhao, L. Lei et al., Deformation Mechanisms in a β-Quenched Ti-5321 alloy: In-Situ Investigation Related to Slip Activity, Orientation Evolution and Stress Induced Martensite, *J. Mater. Sci. Technol.*, 2021, **112**, p 36–48.

20. Bo. Song, YuFu. Wenlong Xiao et al., Role of Nanosized Intermediate Phases on a Precipitation in a High-Strength Near β Titanium Alloy, *Mater. Lett.*, 2020, **275**, 128147

21. B. Song, Y. Chen, W. Xiao et al., Formation of Intermediate Phases and their Influences on the Microstructure of High Strength near-β Titanium Alloy, *Mater. Sci. Eng. A*, 2020, **793**, p 139886.

22. T. Li, M. Lai, A. Kostka, S. Salomon et al., Composition of the Nanosized Orthorhombic O′ Phase and its Direct Transformation to fine α during Ageing in Metastable β-Ti alloys, *Scripta Mater.*, 2019, **170**, p 183–188.

23. R.P. Shi, Y. Zheng, R. Banerjee et al., ω-Assisted α Nucleation in a Metastable β Titanium Alloy, *Scripta Mater.*, 2019, **171**, p 62–66.

24. D.D. Li, W. Wan, L. Zhu et al., Experimental and DFT Characterization of Interphase Boundaries in Titanium and the Implications for ω-Assisted α Phase Precipitation, *Acta Mater.*, 2018, **151**, p 406–415.

25. X.P. Yu and H.B. Dong, Growth Kinetics of α Phase Precipitation in TC21 TITANIUM Alloy during Aging Treatment, *Mater. Mech. Eng.*, 2015, **39**, p 101–105.